EFFECT OF MICROSTRUCTURAL VARIATIONS ON THE FRACTURE TOUGHNESS OF WROUGHT ALLOY 718

W. J. Mills

Westinghouse Electric Corporation
P.O. Box 79
West Mifflin, PA 15122

ABSTRACT

The effect of microstructural variations on the fracture toughness of Alloy 718 was reviewed. The metallurgical parameters surveyed in this paper included heat treatment, heat-to-heat variations, product-form variations, neutron irradiation and long-term thermal aging. Key microstructural features and operative fracture mechanisms were related to macroscopic fracture toughness properties.

INTRODUCTION

Alloy 718 is a high strength superalloy that is used extensively in the aerospace, nuclear and petrochemical industries. Since many of these components are highly loaded during service, fracture control is a primary design concern. This alloy is metallurgically complex involving precipitation of several phases. As a result, the phases present and the resulting fracture toughness can be influenced by heat treatment, processing variables, long-term thermal aging and neutron irradiation. A series of studies were performed at Westinghouse Hanford Company[1-6] to characterize the effects of metallurgical variations on the fracture toughness properties of wrought Alloy 718, and the results are reviewed herein.

SURVEY OF FRACTURE TOUGHNESS VARIATIONS

Effect of Heat Treatment and Heat-to-Heat Variations

The effects of heat treatment and heat-to-heat variations on the J_{IC}[1] and J_R curve responses are summarized in Figure 1. The heat treatments (Table 1) studied were the conventional heat treatment (CHT) per ASTM B637 and the modified heat treatment (MHT) developed by Idaho National Engineering Laboratory[7,8] to improve the impact toughness of Alloy 718 welds. Five different heats and three product forms (plate, forging and bar) from one of these heats are represented in Figure 1. Details of the material supplier, product form and melt practice for these seven material lots are summarized in Table 2. A material lot is defined by a two letter code that designates a particular heat/product form combination. The first letter denotes the heat (A-E) and the second letter denotes the product form (P for plate, B for bar and F for forging). Chemical analyses and tensile properties for the test materials were reported in

[1]All J_{IC} values reported herein were computed using ASTM E813-89 procedures, whereas previously reported values [2-5] were based on ASTM E813-81. The analysis methods were somewhat different for these two versions, so the J_{IC} values reported here differ slightly from those reported earlier.

Superalloys 718, 625 and Various Derivatives
Edited by Edward A. Loria
The Minerals, Metals & Materials Society, 1991

TABLE 1

HEAT TREATMENTS FOR ALLOY 718

Conventional Heat Treatment--CHT (per ASTM B637)

Annealed 1 h at 954°C, air cooled to room temperature
Aged 8 h at 718°C, furnace cooled to 621°C
Held at 621°C for a total aging time of 18 h
Air cooled to room temperature

Modified Heat Treatment--MHT (developed by INEL)

Annealed 1 h at 1093°C, cooled to 718°C at 55°C/h
Aged 4 h at 718°C, cooled to 621°C at 55°C/h
Aged 16 h at 621°C, air cooled to room temperature

References 1-4. The CHT materials exhibited 10-20% higher yield strength levels and 0-10% higher ultimate strength levels, relative to their MHT counterparts. Ductility values were insensitive to heat treatment.

Comparison of the J_R curves for the two heat treatments (CHT on left and MHT on right of Figure 1) on a lot-to-lot basis revealed that the MHT improved the J_{IC} initiation toughness and stable tearing properties for each material. This improvement was most apparent in heats A, B and D, whereas heats C and E displayed only modest increases in fracture properties. It is noted that heats with the highest J_{IC} values also yielded the highest stable tearing resistance. The microstructural features associated with these heat treatment and heat-to-heat variations in toughness behavior are discussed below.

Representative microstructures for the CHT and MHT materials are shown in Figure 2. The MHT alloy had a large grain size as a result of the 1093°C solution anneal that caused substantial grain growth. ASTM grain sizes for the MHT lots ranged from 2 to 4, while those for the CHT lots ranged from 5 to 12. All lots exhibited large niobium-rich and titanium-rich M(C,N)-type carbonitrides. Substantial differences in the density of carbonitrides were observed for the various heats; however, for a given heat the density was independent of heat treatment, because the carbonitrides were unaffected at solution annealing temperatures.

Coarse, lenticular δ (orthorhombic Ni_3Nb) precipitates and a few Laves particles decorated grain boundaries and annealing twins in all CHT lots (Figure 2b). Evidence of intragranular δ particles was also observed in some CHT heats. The MHT, with a 1093°C solution anneal, dissolved the coarse δ and Laves particles in all heats except lot E-B, in which ghost boundaries containing small δ remnants survived.

The nature of the disk-shaped γ" (body-centered tetragonal Ni_3Nb) precipitates, the primary strengthening phase, was also dependent on heat treatment (Figure 2c). The CHT alloys exhibited finer, more closely spaced γ" particles than the MHT alloys.[1] This fine γ" network coupled with the small grain size accounted for the higher strength levels displayed by the CHT alloy.

Fractographic examinations[2-4,6] revealed that the carbonitrides nucleated primary dimples early in the plastic straining process, regardless of heat treatment. Separation of the

TABLE 2

IDENTIFICATION OF ALLOY 718 LOTS

Material Lot	Producer / Heat No.	Product Form	Melt Practice
A-P	Haynes 2180-1-9327	12.7 mm Plate	VIM-ESR
B-B	Teledyne Allvac H-672	15.9 x 41.3 mm Bar	VIM-VAR
C-P	Huntingron 52C9EK	12.7 mm Plate	VIM-ESR
D-F	CarTech 84221	1.6 m Diam. x 66.7 mm Forging	VIM-VAR
E-P	Haynes 2180-6-9457	12.7 mm Plate	VIM-ESR
E-B	Haynes 2180-6-9457	20 mm Diam. Bar	VIM-ESR
E-F	Haynes 2180-6-9457	5:1 Upset Forging	VIM-ESR

ligaments between the primary microvoids then caused the crack to advance. As a result, the secondary cracking mechanism that linked the primary microvoids played an important role in controlling fracture properties. In CHT materials, primary microvoid growth was pre-empted by nucleation of a second microvoid population at the δ particles (Figures 3 and 4). This premature microvoid formation accounted for the relatively low fracture properties displayed by the CHT alloy. In MHT materials, the absence of δ particles enabled the primary dimples to coalesce. Since primary microvoid growth was not interrupted, additional plastic straining was required to advance the crack, thereby resulting in higher J_{IC} and tearing properties.

Heat-to-heat variations in fracture properties were associated with differences in precipitate morphology. In the CHT condition, fracture resistance was related to the inverse of δ phase density. Comparison of the fractographs in Figures 3 and 4 revealed that the inferior fracture resistance for lot D-F (Figure 4), relative to lot B-B (Figure 3), resulted from a particularly high density of δ precipitates. These lenticular particles nucleated an extensive secondary dimple network that caused a low energy advance of the crack.

In most CHT heats, the δ particles, rather than the carbonitrides, controlled fracture behavior. An exception was noted, however, in CHT lot E-B, where the close proximity of primary carbides inside carbide clusters kept the δ particles from participating in the fracture process (Figure 5). Premature failure of these carbide clusters dominated the fracture process and was responsible for the inferior toughness displayed by this lot.

In MHT materials, primary microvoid coalescence was the dominant fracture mechanism. It is not surprising, therefore, that lots containing low carbide densities displayed high fracture resistance and the greatest improvement in fracture properties, relative to their CHT counterparts (Figures 3-5). Figure 6 shows the correlation between carbide density and fracture resistance. Lot B-B, with an exceptionally low carbide density, exhibited the highest toughness; lot A-P, with a low-to-intermediate carbide density, exhibited intermediate toughness; and lot E-B, with an exceptionally high carbide density, exhibited the lowest toughness.

Separation of the ligaments between primary microvoids in the MHT alloy involved three mechanisms: coalescence of primary microvoids; void sheet formation[9,10] associated

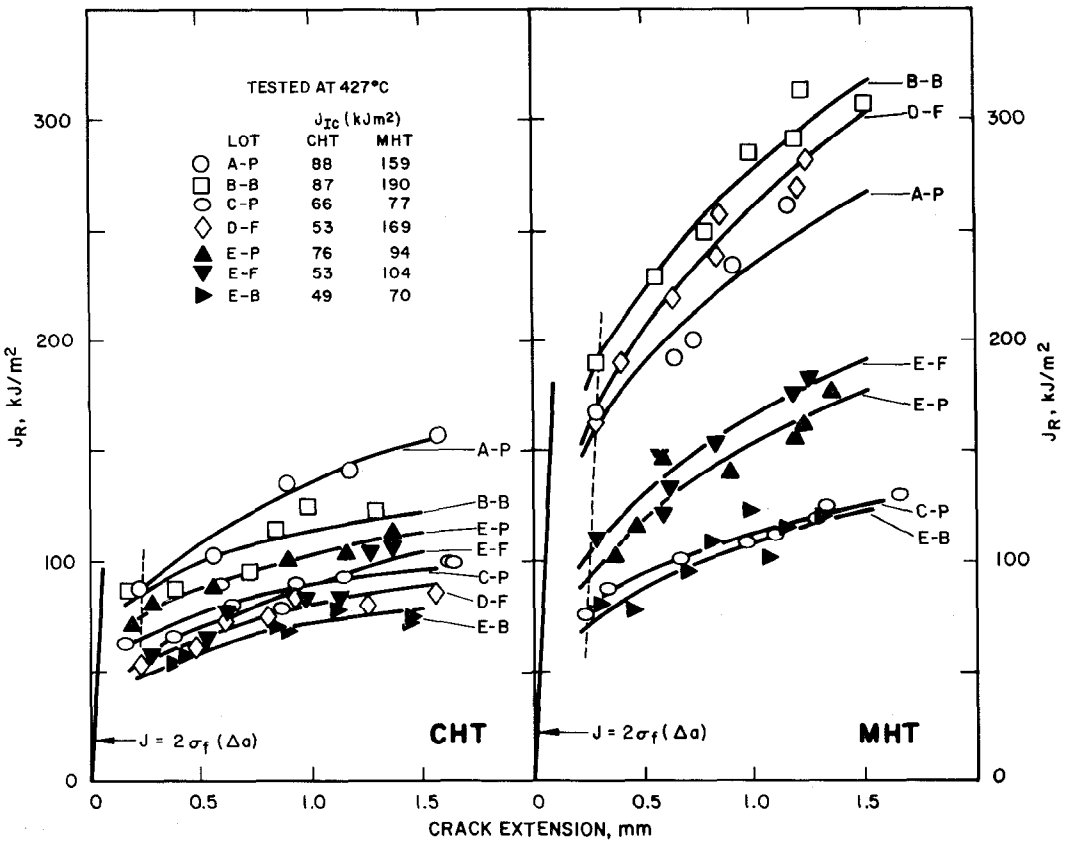

Figure 1. J_R curves for Alloy 718 tested at 427°C. CHT materials are on the left and MHT materials are on the right.

with a fine dimple network nucleated by the γ'' precipitates; and channel fracture[11] associated with localized fracture along planar slip bands. The latter mechanism occurred when dislocation activity was confined to a narrow band of slip planes. Eventually, shear cracks nucleated and propagated along these weakened channels forming a series of steps and ledges that were characteristic of channel fracture. In most heats, the void sheet and channel fracture mechanisms were operative very late in the fracture process as the primary dimples were about to impinge. As a result, these mechanisms did not generally degrade fracture properties. Since primary microvoid growth was not interrupted prematurely, MHT alloys displayed higher J_{IC} values and larger dimples than the CHT alloys. An exception was observed in MHT lot C-P, where channel fracture interrupted microvoid growth (Figure 7). The MHT improved the fracture toughness for this heat as a result of dissolution of δ particles, but the degree of improvement was much less than in most heats, due to the onset of extensive channel fracture.

MHT lot E-B also showed relatively little improvement in toughness over its CHT counterpart. In this lot, the inferior toughness for both heat treated conditions resulted from the presence of carbide clusters that were present in the CHT and MHT materials (Figure 5).

Effect of Temperature

Temperature effects on fracture toughness were found to be dependent on heat treatment. Figure 8 summarizes the J_{IC} response as a function of test temperature for the seven lots discussed in the previous section and for other heats reported in the literature.[12-15] Data for the CHT and MHT alloys are displayed on the left and right, respectively. Statistical

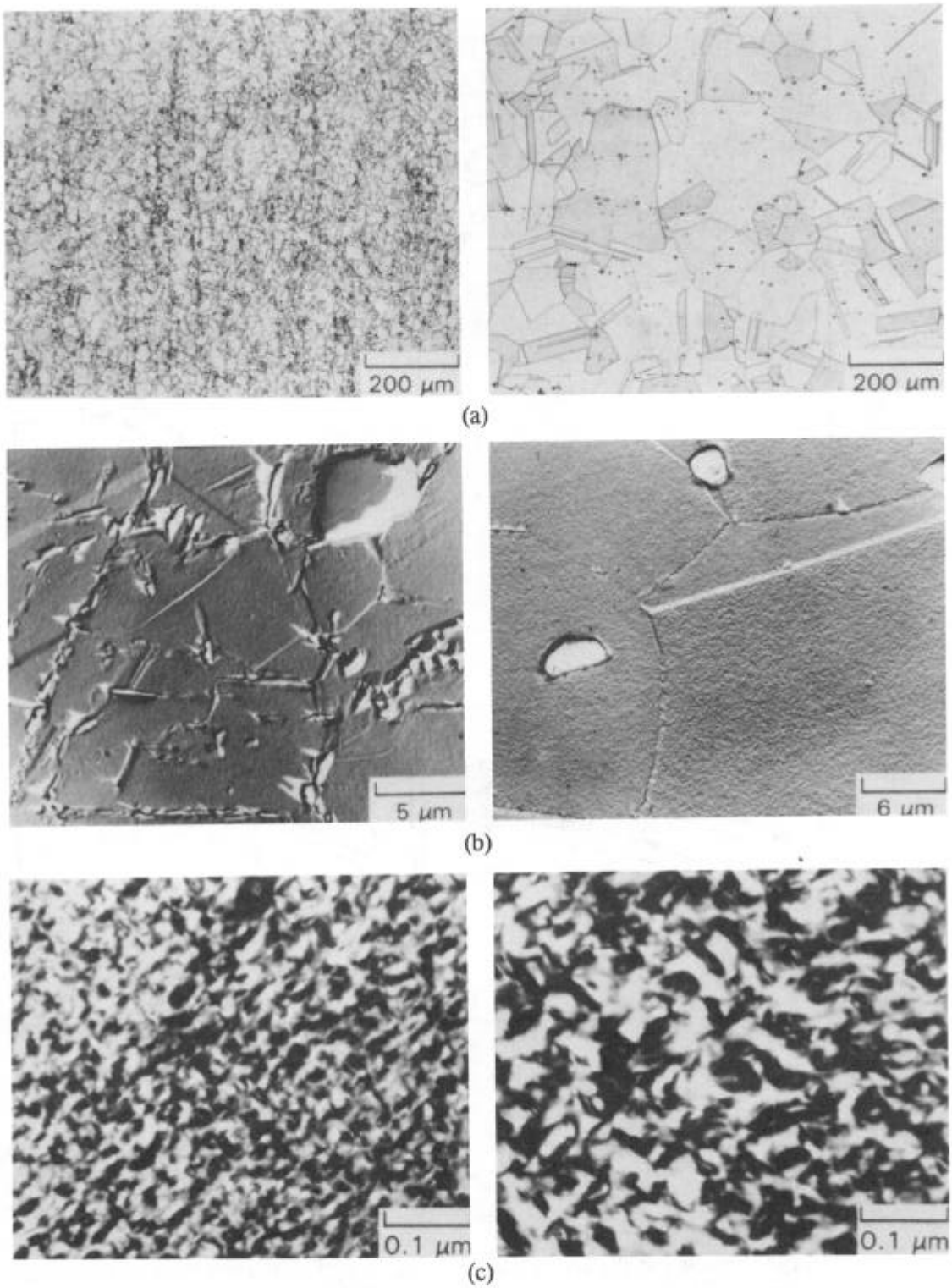

Figure 2. Typical microstructures for Alloy 718. CHT materials are represented on the left; MHT materials are represented on the right.

(a) Light micrographs showing grain size and MC-type carbides.
(b) TEM micrographs of surface replicas taken from polished surfaces.
(c) TEM micrographs of thin foils showing γ'' precipitates.

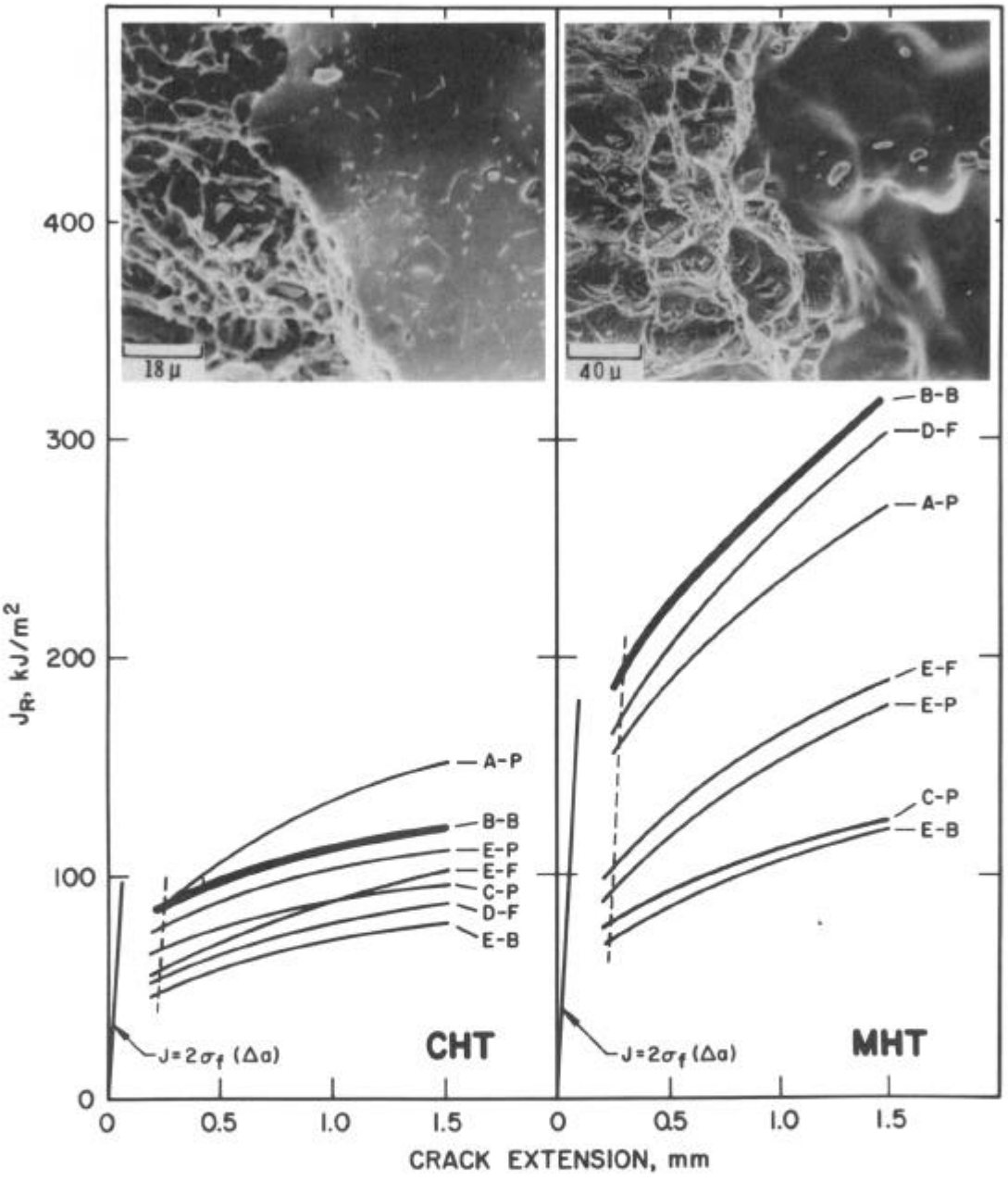

Figure 3. J_R curves for Alloy 718 at 427°C. Typical metallographic-fractographic profiles for CHT and MHT Lot B-B are shown, and J_R curves for these materials are highlighted.

analysis[3,4,6] of the results for the seven lots tested at 24 to 538°C revealed that there were three distinguishable J_{IC} levels for both heat treated conditions. Mean toughness levels for each of these populations are represented by the solid lines on Figure 8. It is seen that the toughness for the CHT material was independent of temperature from 24 to 538°C. Comparison of these results with those obtained by Tobler[12] demonstrated that the temperature-independent behavior continued to -269°C. Figure 8 also revealed that J_{IC} for the MHT material decreased by 20% as the temperature increased from 24 to 538°C.

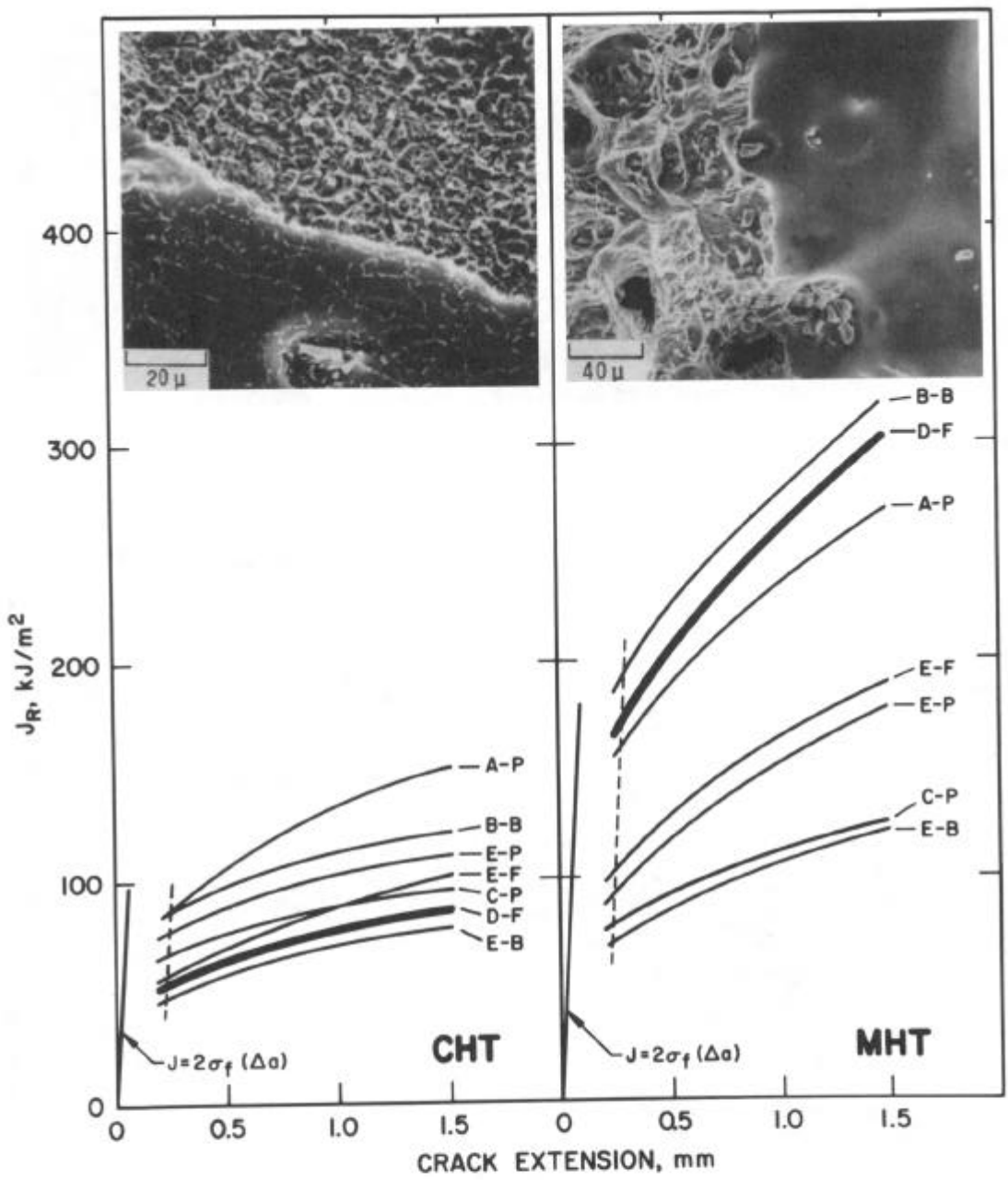

Figure 4. J_R curves for Alloy 718 at 427°C. Typical fractographs for CHT and MHT Lot D-F are shown, and J_R curves for these materials are highlighted.

Effect of Product Form

Comparison of J_{IC} results reported in the literature[6,12-15] revealed no consistent trends with respect to product form for either heat treatment (see Figure 8). Although no consistent trend was observed for the CHT alloy, there was a tendency for plates to exhibit higher fracture resistance than bars and forgings. This probably resulted from the tendency for plates to receive a higher degree of hot working during thermo-mechanical processing. The increased work resulted in superior fracture resistance because it homogenized the alloy and broke down the as-cast second phase network. Exceptions to this trend were noted, however, indicating

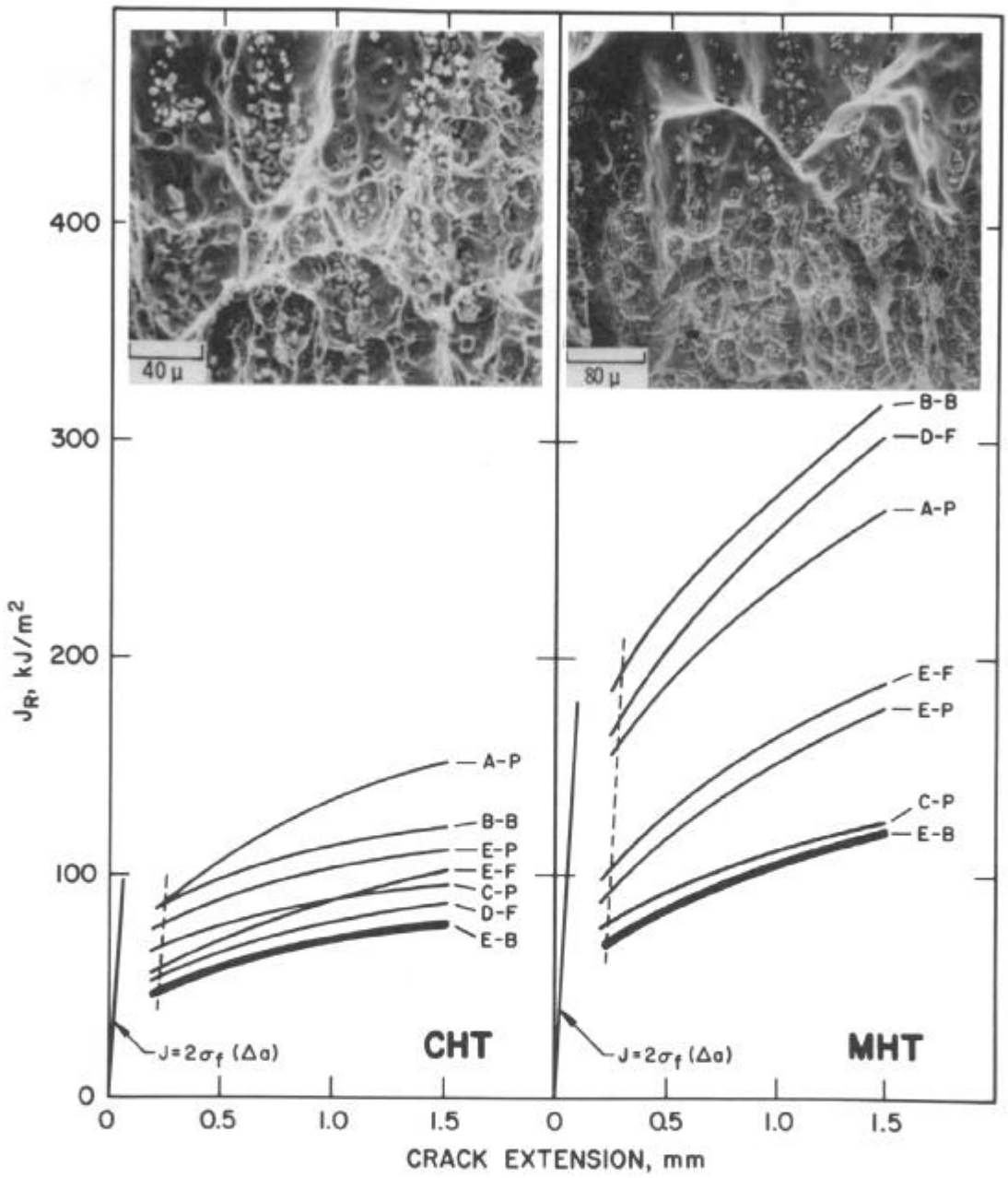

Figure 5. J_R curves for Alloy 718 at 427°C. Typical fractographs for CHT and MHT Lot E-B are shown, and J_R curves for these materials are highlighted.

that while there was a tendency for increased fracture toughness with greater thermo-mechanical working, there was no unique relationship between toughness and product form.

No evidence of product from variations was observed in the MHT material since plates, bars and forgings were contained in both the highest and lowest toughness populations. Thermo-mechanical processing history played an important role in determining the distribution of δ and Laves particles and the degree of segregation in the hot worked product. However, the 1093°C anneal dissolved these particles and homogenized the microstructure, which minimized the influence of processing history. The fracture properties for the MHT materials were controlled by the distribution of carbonitrides, but these particles were not significantly

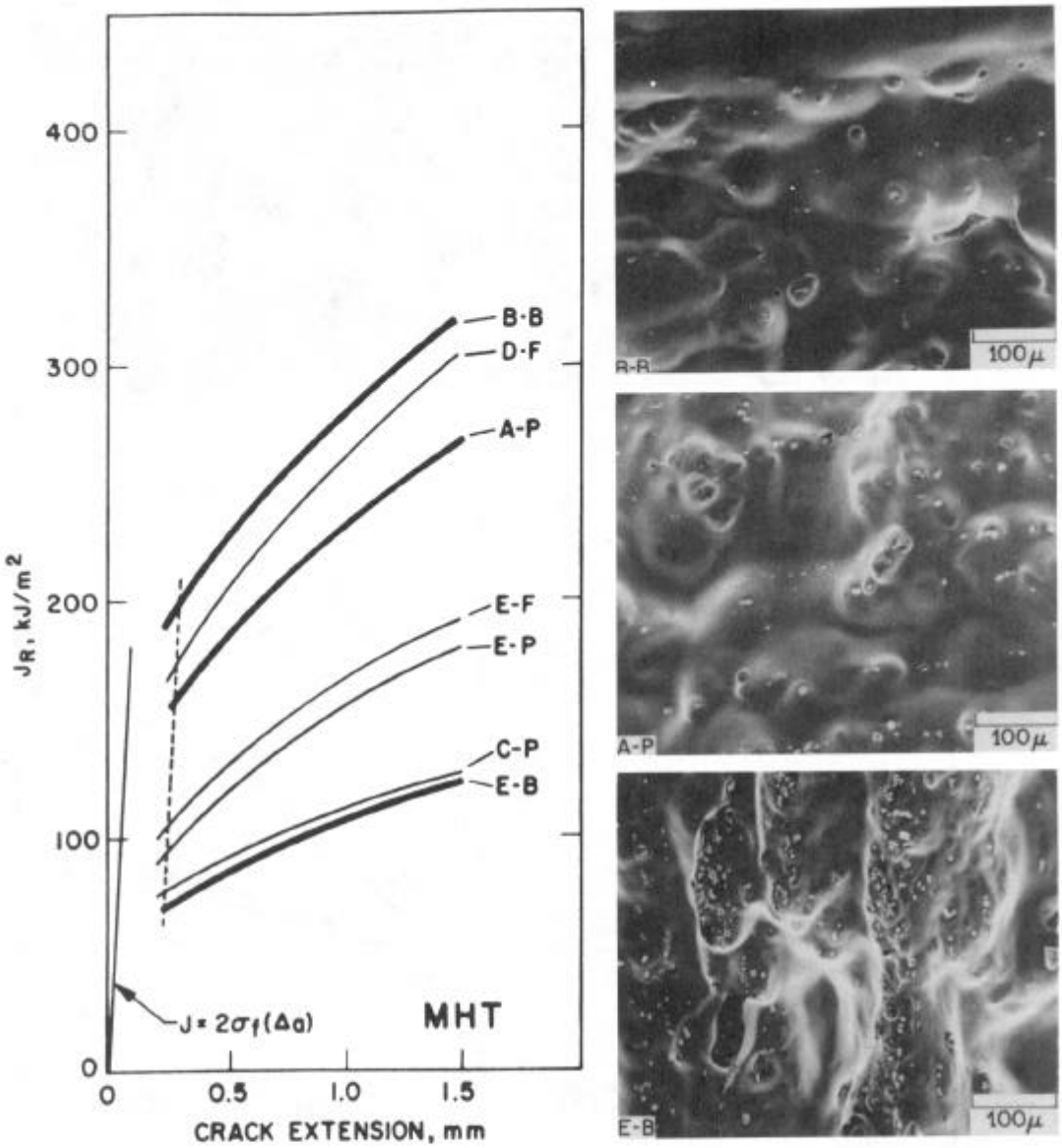

Figure 6. J_R curves for MHT Alloy 718 at 427°C. The carbide morphologies for Lots B-B, A-P and E-B are shown. J_R curves for these lots are highlighted.

affected by hot working. As a result, it is not surprising that product form had a negligible effect on the fracture toughness for MHT materials.

Effect of Thermal Aging

The effect of aging at 566°C for 33,000 hours on the fracture toughness at 538°C is shown in Figure 9. Results for the CHT and MHT alloys are displayed on the left and right, respectively. It is seen that aging caused a 30% to 35% reduction in J_{IC} for both heat treatments. Aging caused a modest reduction in the J_R curve slope for the MHT alloy, but it had no effect on the tearing resistance for the CHT alloy. Fracture toughness testing of the aged material at 24°C revealed comparable trends. Aging at 566°C for 33,000 hours reduced the room temperature J_{IC} from 79 to 55 kJ/m^2 for the CHT alloy and from 125 to 80 kJ/m^2 for the MHT alloy.

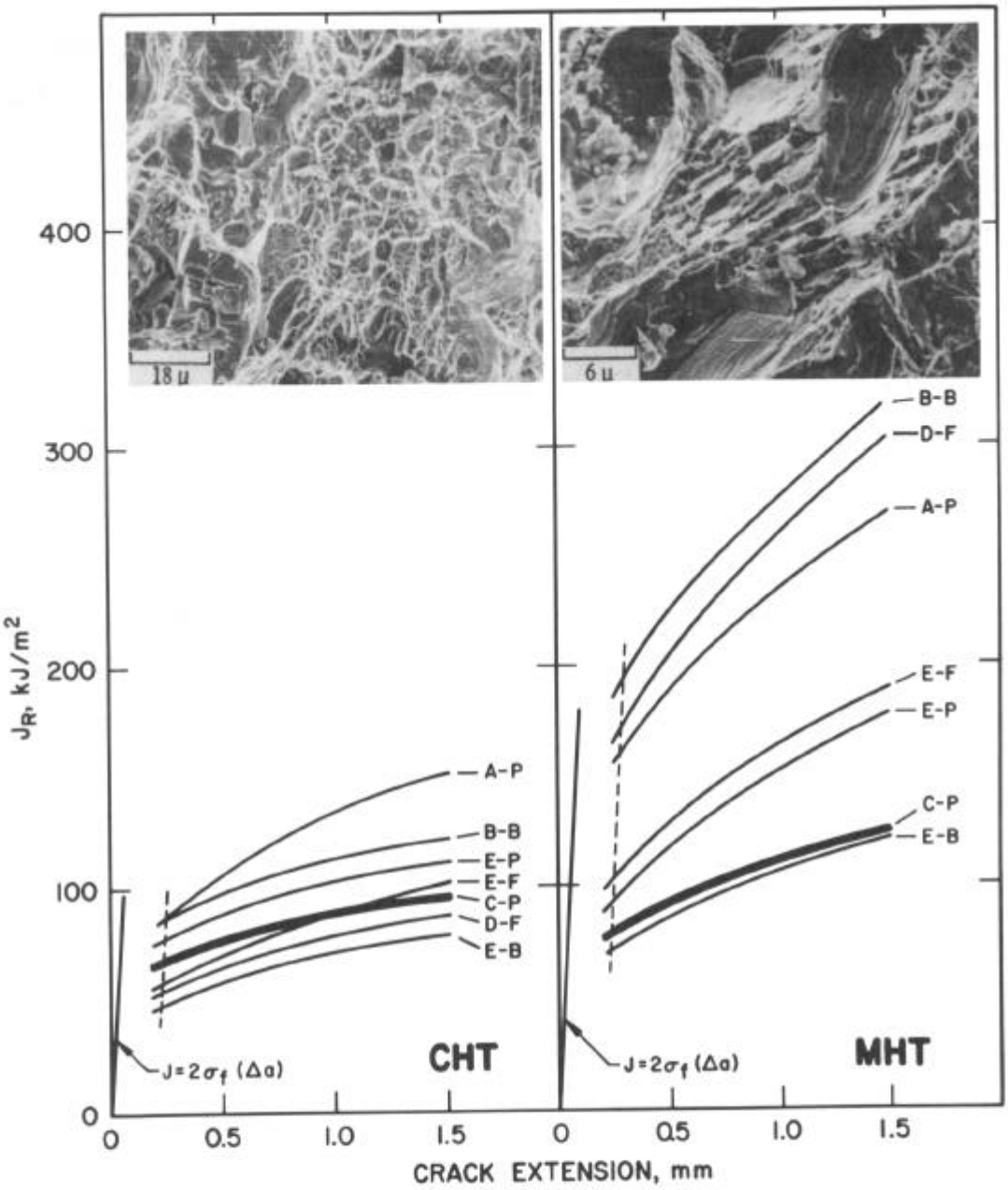

Figure 7. J_R curves for Alloy 718 at 427°C. Typical fractographs for CHT and MHT Lot C-P are shown, and J_R curves for these materials are highlighted.

The post-aging J_{IC} values indicate that the aged alloys were somewhat susceptible to fracture. At these toughness levels, 25-mm thick components possess sufficient constraint to induce plane strain fracture conditions. Critical flaw sizes at stresses equal to half of the yield strength are typically on the order of 10 to 15 mm for the aged CHT alloy and 15 to 20 mm for the aged MHT alloy. Although these crack lengths are relatively large, engineering assessments should be performed to show that critical stress-crack length combinations cannot exist for highly loaded components that are subjected to long-term thermal aging.

The aging-induced degradation in fracture resistance was associated with an increase in matrix strength. Microhardness testing revealed that aging at 566°C for 33,000 hours

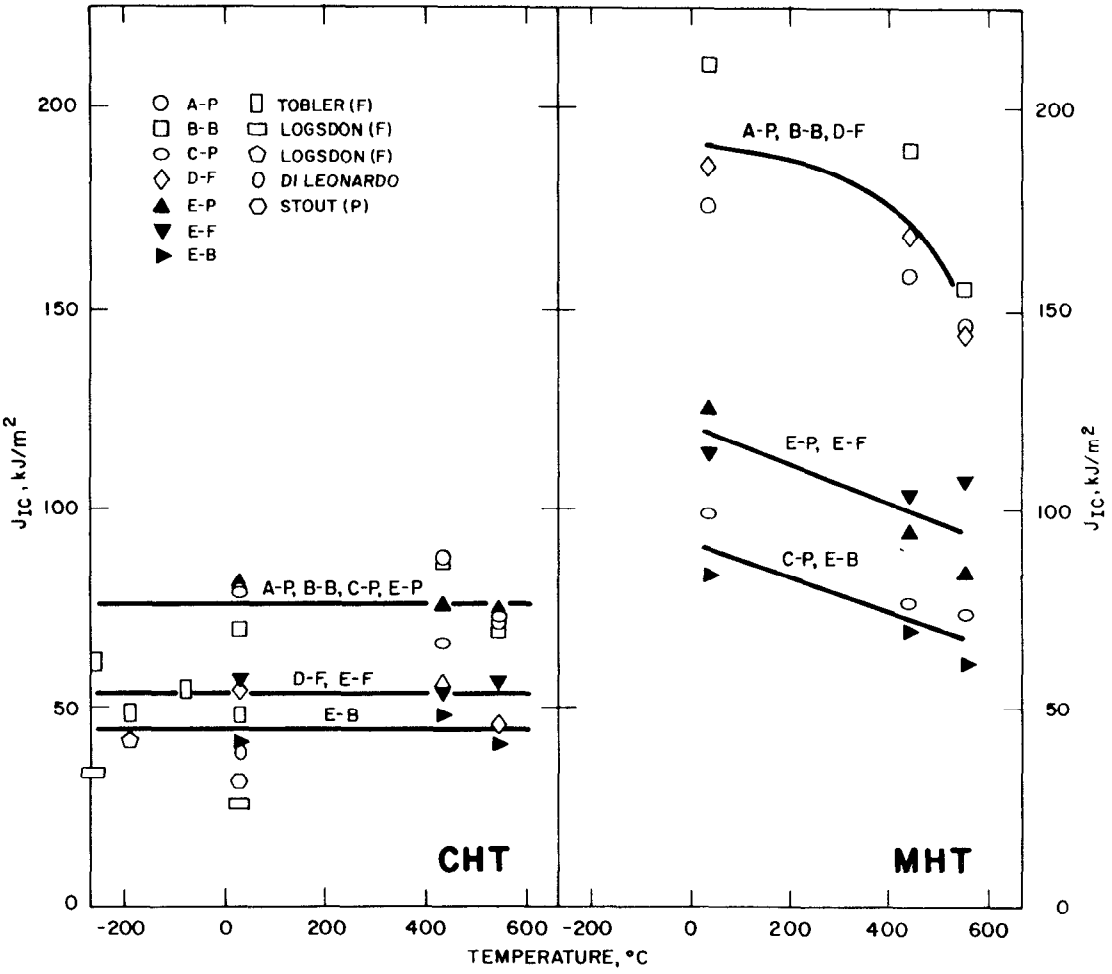

Figure 8. Effect of temperature on J_{IC}.

caused the diamond pyramid hardness (DPH) to increase from 431 $\pm$ 8 to 477 $\pm$ 9 for the CHT matrix and from 433 $\pm$ 8 to 460 $\pm$ 7 for the MHT matrix. The increased strength limited the plastic deformation capabilities, which resulted in the reduction in toughness.

Thermal aging at 566°C had little or no effect on the coarse precipitates for either heat treatment condition (Figure 10a). In the MHT material, aging resulted in the formation of a few, small δ particles along grain boundaries, but these particles were so infrequent and small that they did not influence the overall fracture behavior. In the CHT alloy, the density and morphology of δ particles were essentially unaffected by aging.

The fracture surface appearance for the aged alloys, shown in Figures 10b and 10c, was very similar to that for their unaged counterparts. The aged CHT material exhibited a duplex microvoid coalescence mechanism, with primary microvoids initiating at the large carbonitrides and secondary dimples nucleating at the coarse δ particles. In the MHT alloy, void sheets formed as the primary dimples were about to coalesce; however, since this occurred late in the fracture process, void sheet formation did not have a detrimental effect on fracture toughness. Examination of the metallographic-fractographic profiles for the aged MHT alloy demonstrated that the small intergranular δ precipitates did not participate in the fracture process.

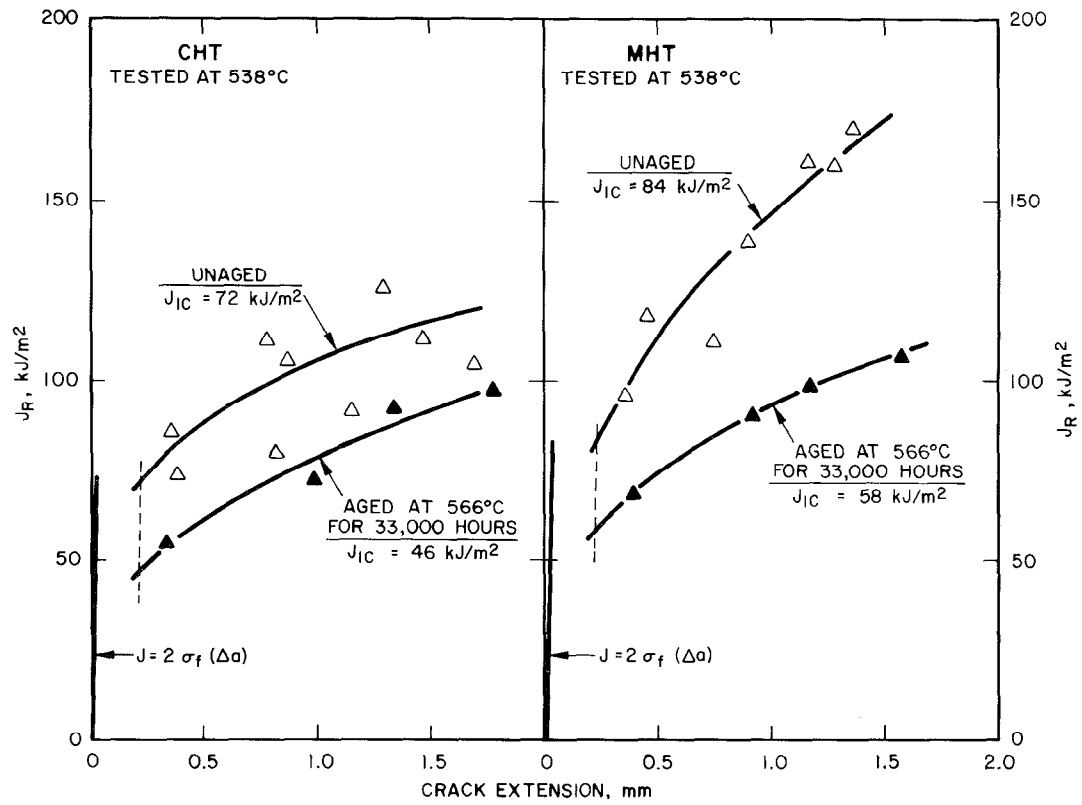

Figure 9. Effect of aging at 566°C for 33,000 hours on the fracture toughness at 538°C. CHT Lot E-P is shown on the left and MHT Lot E-P is shown on the right.

Effect of Neutron Irradiation

The postirradiation J_R curves for CHT and MHT Alloy 718, shown in Figure 11, revealed that neutron irradiation caused a substantial degradation in fracture resistance. Irradiation of the CHT alloy to an exposure of 1.5 dpa resulted in a 30% reduction in J_{IC}, but it had little effect on tearing resistance. At exposures above 8 dpa, fracture properties were independent of irradiation dose, thereby indicating that irradiation embrittlement saturated prior to reaching an exposure of 8 dpa. The CHT alloy exhibited a saturation J_{IC} level that was approximately half of the unirradiated value, whereas the MHT alloy exhibited a 40% degradation in toughness at saturation exposures. The combination of superior unirradiated fracture properties and enhanced irradiation resistance caused the postirradiation toughness for the MHT plate, J_{IC} = 45 kJ/m^2, to be substantially higher than that for its CHT counterpart, J_{IC} = 30 kJ/m^2. Based on these J_{IC} values, critical flaw sizes for stress levels equal to half of the yield strength were typically on the order of 5 to 10 mm and 10 to 15 mm for highly irradiated CHT and MHT components, respectively. These flaw sizes indicate that fracture mechanics analyses, coupled with effective nondestructive evaluation procedures, should be incorporated into structural integrity assessments for highly irradiated components.

Fractographic examinations revealed that the channel fracture mechanism played an important role in the irradiated materials (Figure 12). In the CHT material, irradiation damage promoted planar slip, which resulted in a well-defined channel fracture mechanism that dominated the fracture surface. Lead dislocations swept out irradiation-induced defects and sheared the γ" precipitates, thereby creating channels that were substantially weaker than the surrounding matrix. All subsequent dislocation activity was then confined to these weakened

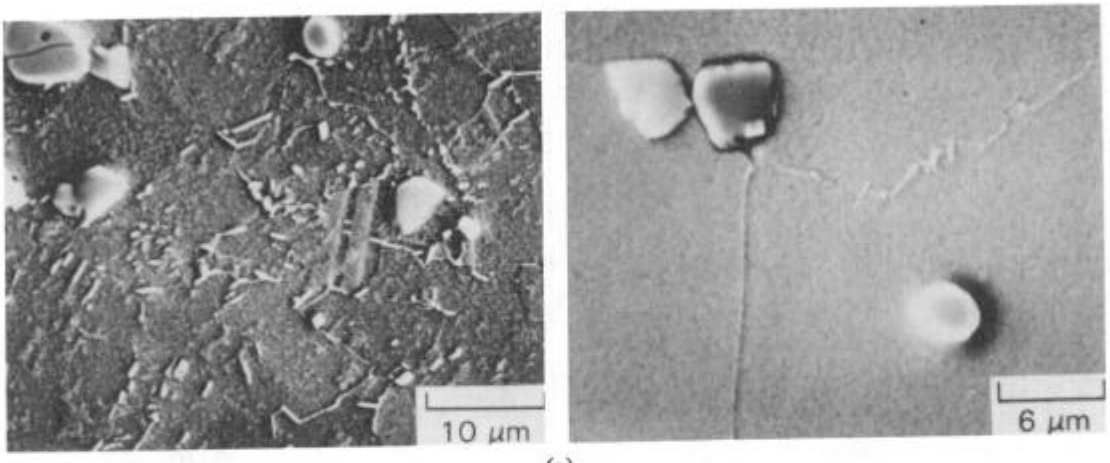

(a)

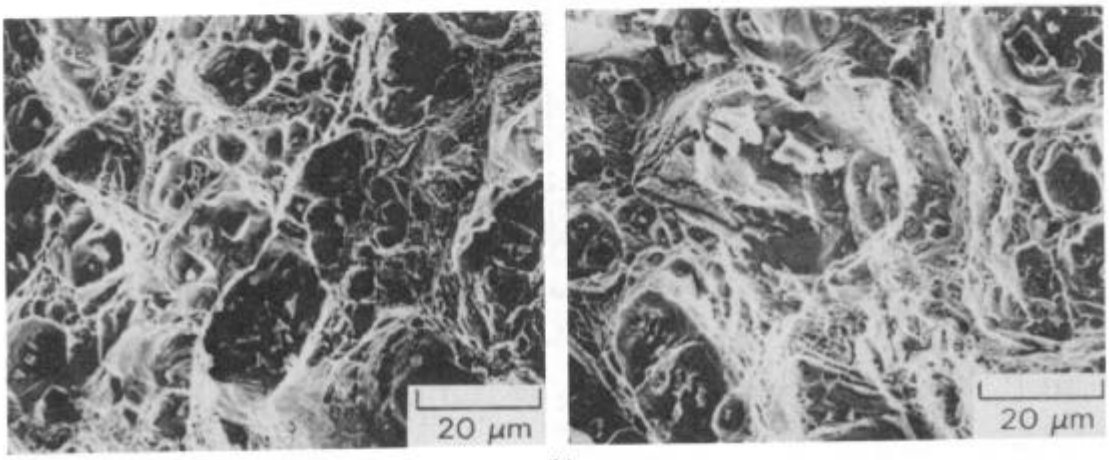

(b)

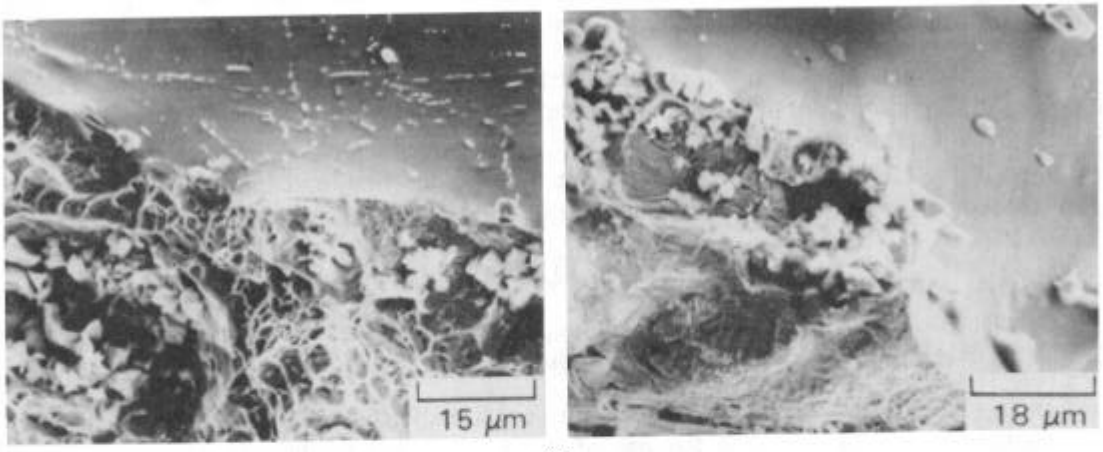

(c)

Figure 10. Typical microstructure and fracture surface appearance for specimens aged at 566°C for 33,000 hours. (CHT alloy on the left; MHT alloy on the right)
(a) SEM micrographs showing grain boundaries and precipitate morphology.
(b) SEM fractographs showing dimple networks.
(c) Metallographic-fractographic profiles showing fracture surface and underlying microstructure.

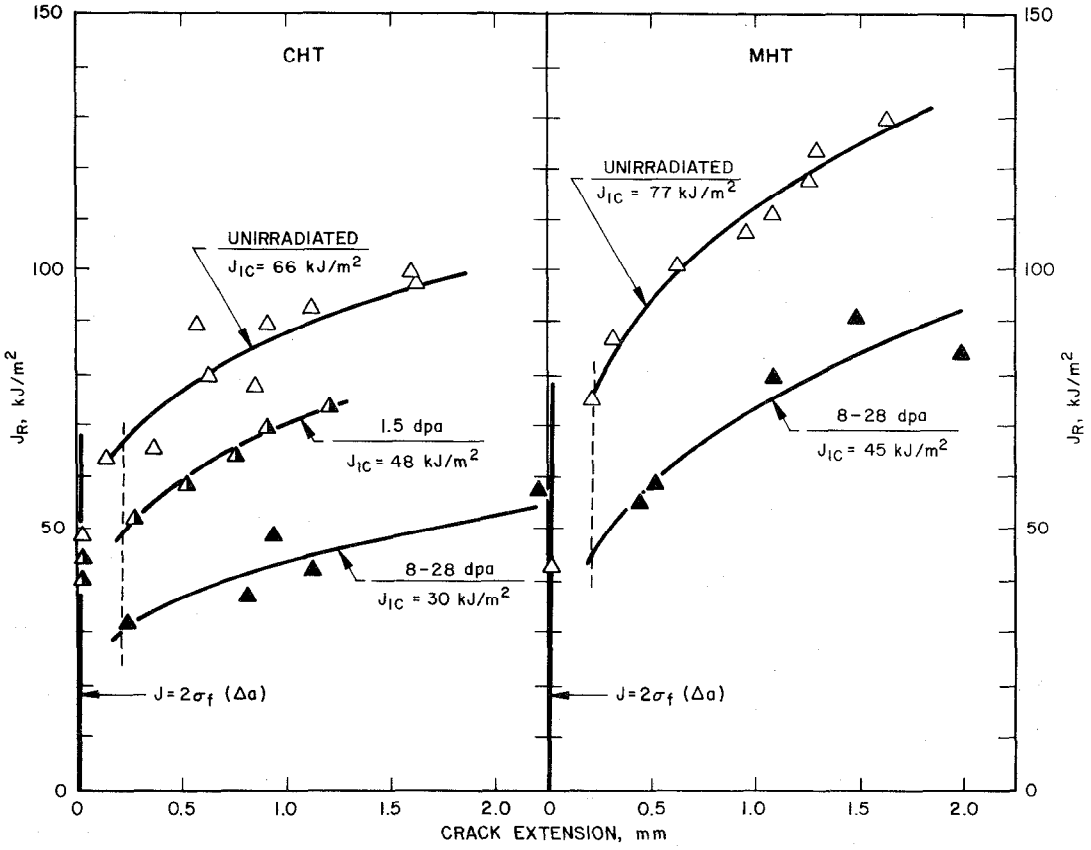

Figure 11. Effect of neutron irradiation on J_R curves at 427°C. CHT Lot C-P is shown on the left and MHT Lot C-P is shown on the right.

channels, ultimately resulting in the channel fracture mechanism. This low energy fracture mechanism resulted in the low fracture resistance displayed by the irradiated CHT alloy.

The irradiated MHT plate exhibited a combination of channel fracture and shallow dimples. Although the dimples were poorly defined, their presence indicated that the matrix possessed limited homogeneous slip capabilities, contrasting the planar slip mechanism that was operative in the CHT alloy. The homogeneous plastic deformation capabilities in the MHT alloy accounted for its superior postirradiation fracture properties.

CONCLUSIONS

The effects of microstructural variations on the fracture toughness behavior of wrought Alloy 718 were reviewed and a summary of the findings is given below.

1. Fracture resistance for the MHT lots was consistently superior to that for their CHT counterparts, which supports the use of the MHT when fracture is a primary design concern. Fracture toughness for the CHT material was found to be independent of temperature, whereas toughness values for the MHT alloy decreased by 20% as temperature increased from 24 to 538°C.

2. Fractographic examinations revealed that primary microvoids nucleated at broken carbonitrides during the initial stages of plastic straining, regardless of heat treatment. The inferior toughness for the CHT alloy was associated with the premature formation of a second population of dimples that were nucleated by coarse δ particles. The MHT anneal

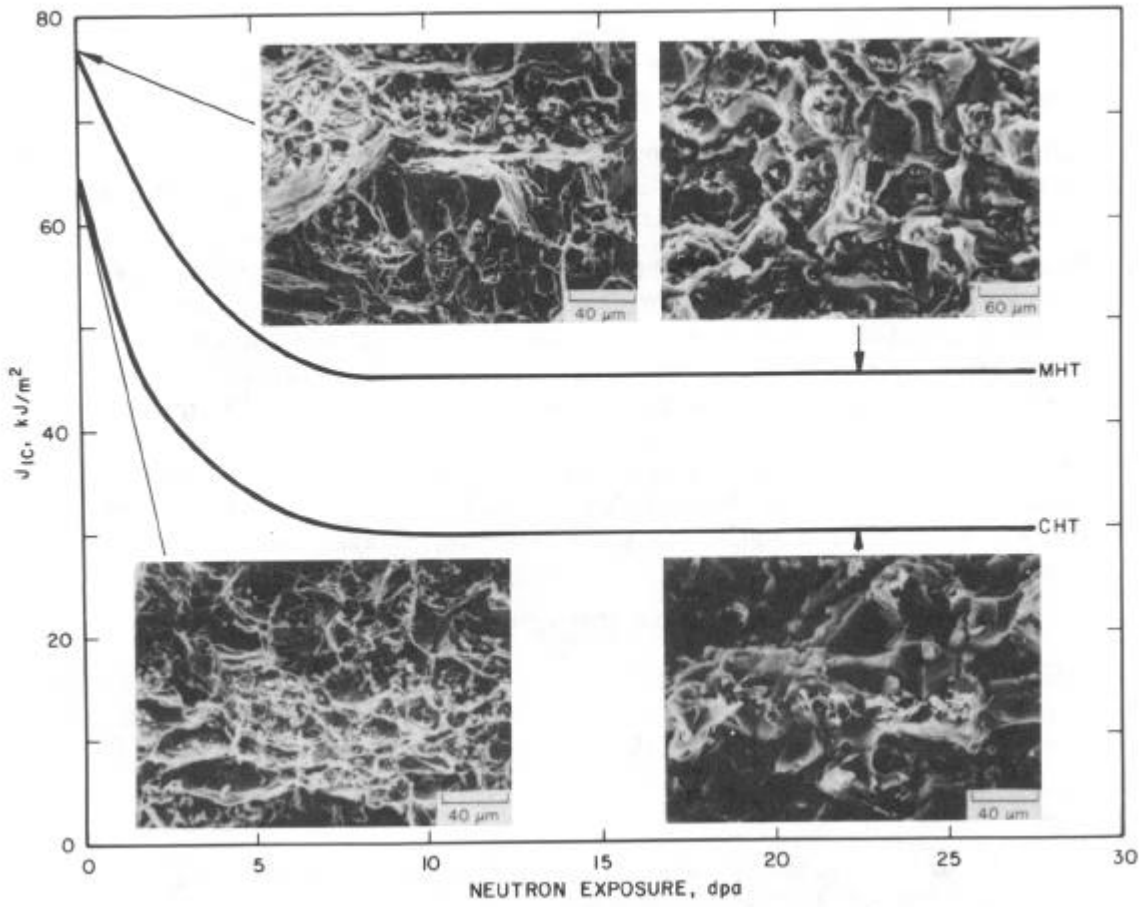

Figure 12. Effect of irradiation on J_{IC}. Fractographs for unirradiated and irradiated Alloy 718 are also shown.

dissolved the coarse δ particles which suppressed secondary microvoid formation and thereby enhanced the fracture resistance.

3. Significant heat-to-heat variations in J_{IC} were observed for both heat treatments. In the CHT material, toughness variations were associated with different microstructures that resulted from differences in thermo-mechanical processing. Materials that received greater thermo-mechanical working tended to exhibit higher J_{IC} values, because the working broke down the as-cast second phase network. By contrast, thermo-mechanical working had little effect on the fracture properties for MHT materials, because the high temperature anneal homogenized the microstructure and minimized the influence of processing history.

4. Heat-to-heat variability was generally attributed to differences in second phase morphology and density. In the CHT alloy, fracture properties were inversely proportional to the density of lenticular δ particles.

5. In MHT materials fracture resistance was inversely proportional to the density of carbonitrides. During the final stages of fracture, primary microvoid growth was sometimes interrupted by void sheet formation or channel fracture. These mechanisms generally occurred as the dimples were about to impinge; hence, they did not necessarily degrade fracture properties. Notable exceptions were observed in the two lowest toughness MHT lots. In these materials, secondary fracture mechanisms prematurely interrupted microvoid coalescence. Extensive channel fracture pre-empted primary dimple growth in

MHT lot C-P, which resulted in its low toughness properties relative to other MHT lots. In MHT lot E-B, the low J_{IC} values were associated with a very high density of carbo-nitrides and a secondary dimple population nucleated by δ particle remnants.

6. Aging at 566°C for 33,000 hours caused a 30% reduction in J_{IC} at 24 and 538°C for both the CHT and MHT materials. The toughness degradation was caused by an increase in matrix strength, which limited plastic deformation capabilities.

7. Neutron irradiation significantly degraded J_{IC} for both heat treatment conditions. The toughness degradation saturated prior to an exposure of 8 dpa. Irradiation to saturation exposures caused a 50% reduction in J_{IC} for the CHT material and a 40% reduction in J_{IC} for the MHT material. Channel fracture was dominant in the irradiated CHT material as all dislocation activity was channeled through narrow slip bands. The transition from homogeneous to heterogeneous slip resulted in the low fracture resistance exhibited by the irradiated CHT alloy. The irradiated MHT alloy displayed a combination of channel fracture and poorly defined dimples. The presence of dimples indicated that the MHT matrix possessed limited homogeneous slip capabilites, which accounted for its superior postirradiation fracture resistance.

REFERENCES

1. Mills, W. J., "The Influence of Heat-Treatment on the Microstructure and Mechanical Properties of Alloy 718 Base Metal and Weldments," Report HEDL-TME 78-54, Westinghouse Hanford Company, Richland, WA, 1979.
2. Mills, W. J., Journal of Engineering Materials and Technology, Vol. 102, 1980, pp. 118-126.
3. Mills, W. J. and Blackburn, L. D., Journal of Engineering Materials and Technology, Vol. 110, 1988, pp. 286-293.
4. Mills, W. J. and Blackburn, L. D., Journal of Engineering Materials and Technology, Vol. 112, 1990, pp. 116-123.
5. Mills, W. J., "Effect of Irradiation on the Fracture Toughness of Alloy 718 Plate and Weld," Accepted for publication in Journal of Nuclear Materials.
6. Mills, W. J., Superalloy 718--Metallurgy & Applications, 1989, pp. 517-532.
7. Smolik, G. R. and Reuter, W. G., "Heat Treatment Versus Properties Studies Associated with Inconel 718 PBF Acoustic Filters," Technical report No. 493, Aerojet Nuclear Company, Idaho Falls ID, 1975.
8. Reuter, W. G., "Design Data for the 1/4-in. Thick Alloy 718 In-Pile Tube," Report TREE-NUREG-1087, EG&G Idaho, Inc., Idaho Falls, ID, 1977.
9. Rogers, H. C., Ductility, ASM, Metals Park, OH, 1968, pp. 31-61.
10. Cox, T. B. and Low, J. R., Jr., Metallurgical Transactions, Vol. 5, 1974, pp. 1457-1470.
11. Hunter, C. W., Fish, R. L. and Holmes, J. J., Transactions of the American Nuclear Society, Vol. 15, 1972, pp. 254-255.
12. Tobler, R. L., Cryogenics, Vol. 16, 1976, pp. 669-674.
13. Logsdon, W. A., Kossowsky, R. and Wells, J. M., Advances in Cryogenic Engineering, Vol. 24, 1978, pp. 197-209.
14. Stout, M. G. and Gerberich, W. W., Metallurgical Transactions, Vol. 9A, 1978, pp. 649-658.
15. Di Leonardo, G., International Journal of Fracture, Vol. 20, 1982, pp. 313-323.